Rare Metal Materials and Engineering
Volume 55, Issue 1, January 2026
Available online at www.rmme.ac.cn

Science Press

Cite this article as: Li Suli, Zhang Yanze, Yang Mengjia, et al. Effect of Addition of Er-TiB_2 Dual-Phase Nanoparticles on Strength-Ductility of Al-Mn-Mg-Sc-Zr Alloy Prepared by Laser Powder Bed Fusion[J]. Rare Metal Materials and Engineering, 2026, 55(01): 9-17. DOI: https://doi.org/10.12442/j.issn.1002-185X.20250085.

ARTICLE

Effect of Addition of Er-TiB_2 Dual-Phase Nanoparticles on Strength-Ductility of Al-Mn-Mg-Sc-Zr Alloy Prepared by Laser Powder Bed Fusion

Li Suli[1], Zhang Yanze[1], Yang Mengjia[1], Zhang Longbo[1], Xie Qidong[2], Yang Laixia[1], Mao Feng[3], Chen Zhen[2]

[1] School of Mechanical Engineering, Xi'an University of Science and Technology, Xi'an 710054, China; [2] School of Mechanical Engineering, Xi'an Jiaotong University, Xi'an 710049, China; [3] Longmen Laboratory, Luoyang 471000, China

Abstract: A dual-phase synergistic enhancement method was adopted to strengthen the Al-Mn-Mg-Sc-Zr alloy fabricated by laser powder bed fusion (LPBF) by leveraging the unique advantages of Er and TiB_2. Spherical powders of 0.5wt% Er-1wt% TiB_2/Al-Mn-Mg-Sc-Zr nanocomposite were prepared using vacuum homogenization technique, and the density of samples prepared through the LPBF process reached 99.8%. The strengthening and toughening mechanisms of Er-TiB_2 were investigated. The results show that Al_3Er diffraction peaks are detected by X-ray diffraction analysis, and texture strength decreases according to electron backscatter diffraction results. The added Er and TiB_2 nano-reinforcing phases act as heterogeneous nucleation sites during the LPBF forming process, hindering grain growth and effectively refining the grains. After incorporating the Er-TiB_2 dual-phase nano-reinforcing phases, the tensile strength and elongation at break of the LPBF-deposited samples reach 550 MPa and 18.7%, which are 13.4% and 26.4% higher than those of the matrix material, respectively.

Key words: Al-Mn-Mg-Sc-Zr alloy; laser powder bed fusion; nano-reinforcing phase; synergistic enhancement

1 Introduction

Aluminum alloys are critical structural materials renowned for their high strength-to-weight ratio, superior impact resistance, excellent ductility, and corrosion resistance, making them widely used in the aerospace industry[1–2]. Laser powder bed fusion (LPBF) technique significantly improves material utilization, reduces manufacturing cycles, and lowers costs. A distinctive feature of LPBF is its ability to rapidly melt metal powders via a laser beam, followed by immediate solidification, achieving cooling rates of $10^4 – 10^6$ K/s. This rapid cooling characteristic, driven by large temperature gradients, leads to significant refinement in the alloy's microstructure[3]. Moreover, under such fast-cooling conditions, the ultimate solid solubility of alloying elements increases markedly, enabling the formation of a supersaturated solid solution with a solubility far exceeding the equilibrium solid solubility of the alloying elements, and thereby improving the mechanical properties of the components.

Currently, most researches on LPBF-fabricated aluminum alloys are confined to Al-Si and Al-Mg-Si systems. Although these alloys can effectively reduce product mass, their strength and toughness are insufficient to meet the final

Received date: February 20, 2025
Foundation item: Shaanxi Province Qin Chuangyuan "Scientist+Engineer" Team Construction Project (2022KXJ-071); 2022 Qin Chuangyuan Achievement Transformation Incubation Capacity Improvement Project (2022JH-ZHFHTS-0012); Shaanxi Province Key Research and Development Plan-"Two Chains" Integration Key Project-Qin Chuangyuan General Window Industrial Cluster Project (2023QCY-LL-02); Xixian New Area Science and Technology Plan (2022-YXYJ-003, 2022-XXCY-010); 2024 Scientific Research Project of Shaanxi National Defense Industry Vocational and Technical College (Gfy24-07); Shaanxi Vocational and Technical Education Association 2024 Vocational Education Teaching Reform Research Topic (2024SZX354); National Natural Science Foundation of China (U24A20115); 2024 Shaanxi Provincial Education Department Service Local Special Scientific Research Program Project-Industrialization Cultivation Project (24JC005, 24JC063); Shaanxi Province "14th Five-Year Plan" Education Science Plan, 2024 Project (SGH24Y3181); National Key Research and Development Program of China (2023YFB4606400); Longmen Laboratory Frontier Exploration Topics Project (LMQYTSKT003)
Corresponding author: Chen Zhen, Ph. D., Associate Professor, School of Mechanical Engineering, Xi'an Jiaotong University, Xi'an 710049, P. R. China, E-mail: chenzhen2025@xjtu.edu.cn

application requirements as key materials for complex functional components in aerospace vehicles[4]. The 2xxx and 7xxx series aluminum alloys have wide solidification intervals and high hot cracking susceptibility, posing significant challenges to forming during laser additive manufacturing[5]. In comparison, the Al-Mn-Mg-Sc-Zr has relatively balanced overall performance. However, its tensile strength is still rather low, failing to meet the performance requirements of the aerospace field. This is attributed to its relatively high laser reflectivity and thermal conductivity, necessitating higher laser energy input. Consequently, this leads to poor forming stability and considerable fabrication difficulties[6–7].

Li et al[8] prepared TiB_2/$AlSi_{10}Mg$ specimens by LPBF, which significantly improved the tensile strength and tensile strain of the formed parts. The tensile strength reached 530± 16 MPa, and the elongation reached 15.5%±1.2%, making this alloy an aluminum matrix composite formed by LPBF with relatively high comprehensive mechanical properties. Shi et al[9] investigated the influence of element Er on the microstructure of aluminum alloys. Through optimization of process parameters and adjustment of heat treatment, they increased the tensile strength from 415.2 MPa to 524.4 MPa. Martin et al[10] from HRL Laboratory (USA) coated 7075Al powder particles with nanoparticles such as TiB_2, ZrH_2, and WC. The addition of these nanoparticles inhibited the hot cracking tendency during the LPBF process, enabled the transformation from columnar to equiaxed grains, and reduced material anisotropy. Wang et al[11] prepared Ti+B_4C/AA7075 composite powder by high-energy ball milling, increasing its tensile strength from 200.1 MPa to 336.9 MPa.

Studies have demonstrated that the rare earth element Er has a strong modifying effect. Similar to Al_3Sc, the primary phase Al_3Er has good interfacial coherence with the Al matrix, enabling it to act as a non-homogeneous nucleation core to greatly improve the nucleation rate. In addition, fine Al_3Er particles can pin dislocations and subgrain boundaries, hindering dislocation aggregation and migration at subgrain boundaries, thus delaying the nucleation and growth of subgrains[12]. The laser reflectivity of ceramic particles is much lower than that of aluminum alloys, so TiB_2 is used as a reinforcing phase to strengthen aluminum alloys. When uniformly attached to the surface of the aluminum matrix, TiB_2 improves the laser absorption capacity of aluminum alloys, resulting in better LPBF formability[13].

In this research, a dual-phase synergistic reinforcement approach using Er and TiB_2 was employed to enhance the Al-Mn-Mg-Sc-Zr alloy, leveraging the respective strengthening advantages of Er and TiB_2. It is expected that the dual-phase reinforcement of rare earth elements and ceramic particles will provide a new insight into the formation of novel aluminum matrix composites by LPBF.

2 Experiment

The powder used in this experiment was Al-4.88Mn-1.66Mg-0.69Sc-0.33Zr, developed by Suzhou Beifeng Technology, with a particle size range of 15–53 μm. The selected Er powder had a particle size of 1 μm and the TiB_2 powder had a particle size of 100 nm. 1wt% TiB_2 particles and 0.5wt% Er powder were mixed with the Al-Mn-Mg-Sc-Zr alloy by vacuum homogenization method. The vacuum homogenizer ZYMC-200V was used. The morphology and particle size of the maxed composite powder are shown in Fig.1a and Fig.1b, respectively.

The LPBF device used in this study was SLM100-N2, independently developed by Xi'an Jiaotong University. Cubic sample of 8 mm×8 mm×8 mm was printed under the constant parameters: laser power of 400 W, scanning speed of 1000 mm/s, hatch spacing of 100 μm, and layer thickness of 30 μm. In the LPBF process, the oxygen content in the forming chamber was controlled within 10^5 μg/L to prevent high-temperature oxidation of the material.

JEM-IT500 tungsten filament scanning electron microscope (SEM), manufactured by JEOL Ltd, Japan, was used to observe the microscopic morphology of the samples in detail. Phase analysis of the samples was performed using a transmission electron microscope (TEM), an energy disperse sectroscope (EDS), and a Bruker D8 ADVANC X-ray diffractometer (XRD, Germany) within scanning range of 10°–90° . The acquired diffraction data were processed and analyzed using MDI JADE6.0 software. The grain size, orientation, and texture of the samples were analyzed by electron backscatter diffraction (EBSD) using a JSM-7900F field emission SEM manufactured by JEOL Ltd, Japan. The EBSD data were then processed using Channel 5 software. The mechanical properties of the samples were tested by

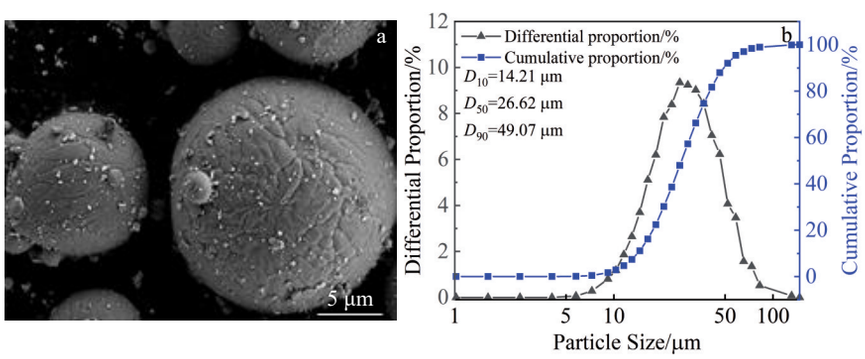

Fig.1 Morphology (a) and particle size distribution (b) of Er-TiB_2/Al-Mn-Mg-Sc-Zr powder

tensile test on an Instron M4206 machine at a strain rate of 1 mm/min, according to GB/T 228.1-2010 standard.

3 Results and Discussion

3.1 Phase analysis

Fig. 2 shows XRD patterns of the Al-Mn-Mg-Sc-Zr alloy and Er-TiB_2/Al-Mn-Mg-Sc-Zr composite samples. It can be seen that the diffraction peak of Al (111) is significantly enhanced and becomes more intense than that of Al (200) after the addition of the reinforcing phases. This phenomenon occurs because TiB_2 has excellent thermal conductivity, enabling more efficient heat transfer from the center of the molten pool to its surrounding areas, making the temperature distribution in the molten pool more uniform, and thus optimizing the temperature gradient[14]. The optimized temperature gradient will guide the grain growth along the direction of heat flow. Since the (111) crystal plane is the most densely packed plane of Al atoms, under the appropriate temperature gradient conditions, Al atoms are more inclined to nucleate on the surface of TiB_2 particles with the (111) crystal plane, thereby increasing the nucleation rate of the (111) crystal plane. In terms of phase composition, only the fcc-Al phase is observed in the Al-Mn-Mg-Sc-Zr alloy, while the diffraction peak of Al_3Sc is detected in the Er-TiB_2/Al-Mn-Mg-Sc-Zr alloy, indicating that Al_3Sc phase particles are generated in the composite sample. Additionally, TiB_2 is detected, and no other Ti-containing compounds are detected, indicating that TiB_2 does not react with the Al matrix. The diffraction peak of Al_3Er is also detected in the composite, which indicates that the reaction of Al and Er generates the Al_3Er phase.

3.2 Microstructure analysis

According to EBSD image of the Al-Mn-Mg-Sc-Zr alloy (Fig. 3a), it can be seen that the Al-Mn-Mg-Sc-Zr alloy prepared by LPBF is mainly composed of columnar grains growing along the forming direction, with small equiaxed grains present at the molten pool boundaries. Fig. 3b shows that the columnar grain region is significantly reduced after the addition of the reinforcing phases. The columnar crystal size decreases, and the equiaxed grain region increases significantly and becomes denser near the molten pool boundary. This is because TiB_2 and Er are uniformly distributed in the matrix to form a dispersed phase, which inhibits the grain growth[15]. Al_3Er phase is formed in the LPBF process, exhibiting good interfacial coherence with the matrix. The melting point of Al_3Er is much higher than that of the matrix powder, so Al_3Er remains solid once formed, and acts as a heterogeneous nucleation site during melt crystallization, preventing the flow of the molten pool, hindering grain growth, and thus further enhancing the grain refinement effect.

It can be seen from Fig.4a and 4b that both alloys exhibit a certain degree of texture. Specifically, the orientation strength of Al-Mn-Mg-Sc-Zr alloy in the [001] direction reaches 4.80 multiple of random distribution (mrd). After the addition of Er and TiB_2, the maximum texture strength is lower than 2.99 mrd, the texture is weakened, and the polar intensity distribution is very uniform. This indicates that the addition of nanoparticles can eliminate the anisotropy caused by temperature gradient during the LPBF process, thereby enhancing the

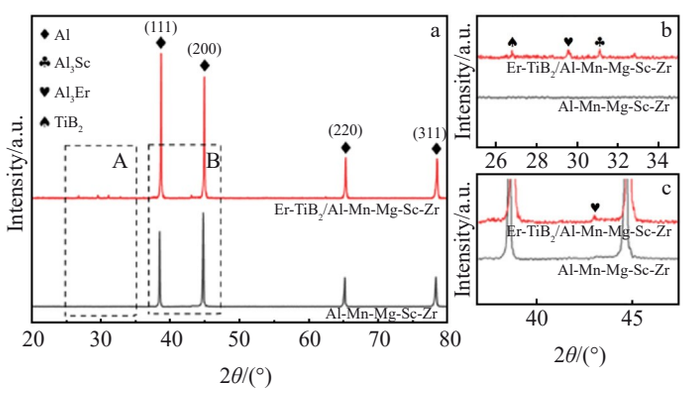

Fig.2 XRD patterns of formed samples: (a) overall patterns; (b) magnified patterns of area A; (c) magnified patterns of area B

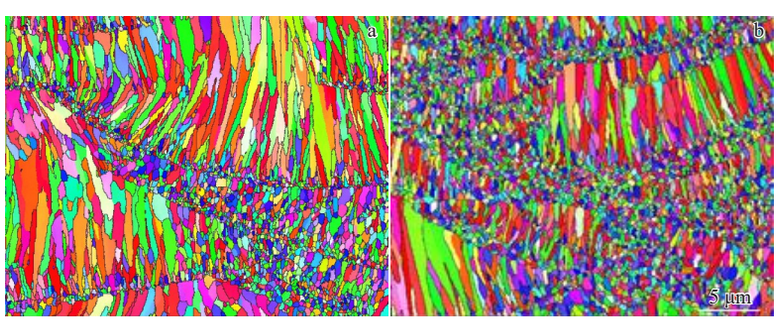

Fig.3 EBSD images of Al-Mn-Mg-Sc-Zr (a) and Er-TiB_2/Al-Mn-Mg-Sc-Zr (b) samples

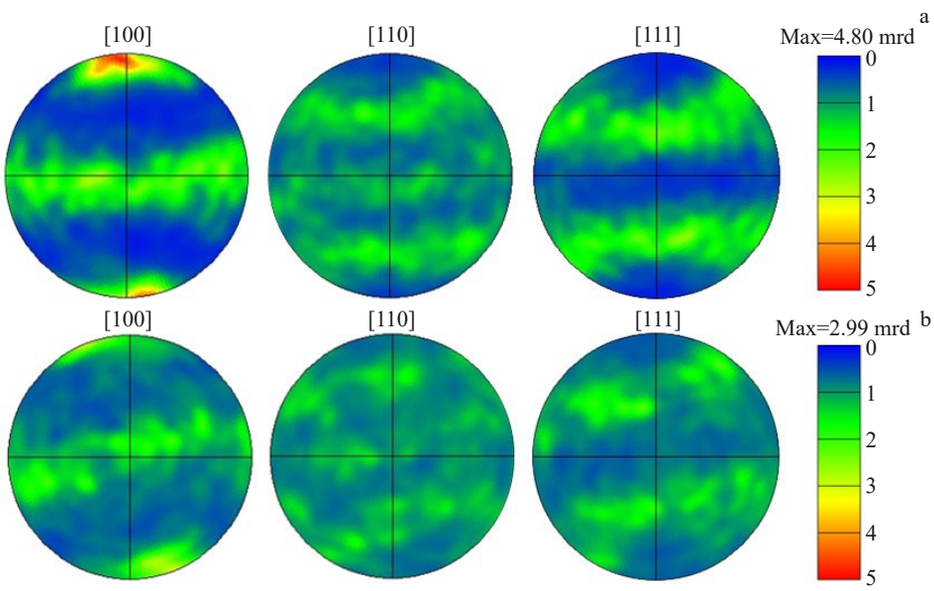

Fig.4 EBSD pole diagrams of Al-Mn-Mg-Sc-Zr (a) and Er-TiB_2/Al-Mn-Mg-Sc-Zr (b) samples

multi-directional grain growth. Consequently, the material will display more uniform mechanical behavior under stress in different directions, and it will be less prone to brittle fracture[9].

Fig. 5 shows TEM analysis results of 0.5wt% Er-1wt%

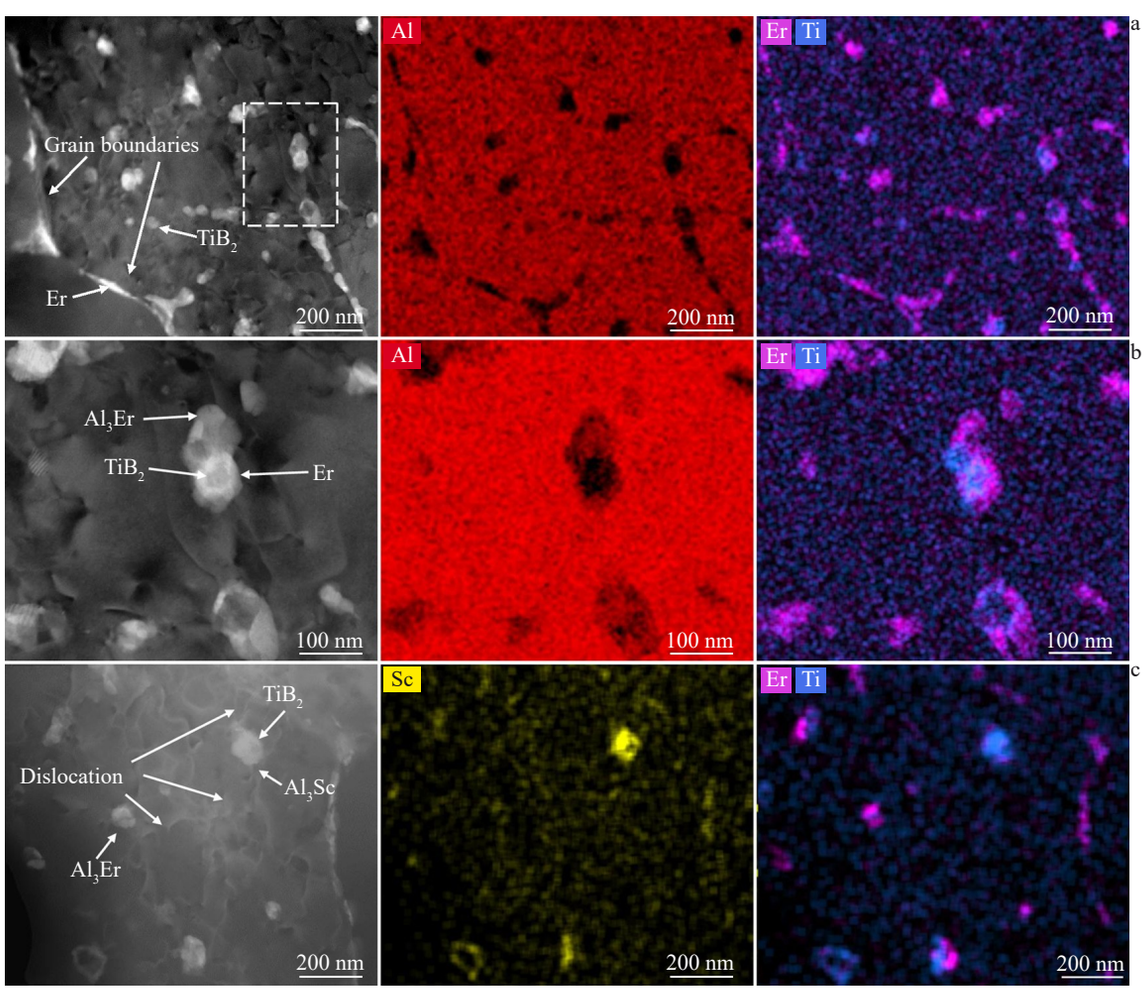

Fig.5 TEM images and corresponding EDS mappings of Al_3Er, TiB_2, and Er (a, c); magnified TEM image and corresponding EDS mappings of dotted area in Fig.5a (b)

TiB_2/Al-Mn-Mg-Sc-Zr alloy. It can be seen from Fig. 5a that Er and TiB_2 are distributed both inside the grains and at the grain boundaries. As shown in Fig. 5b, Er and TiB_2 are co-distributed in the composite matrix, and TiB_2 is attached to Er-containing structure, which has a stabilization effect on the Er while stabilizing the matrix structure. The spherical Al_3Er phases can be found, indicating that element Er exists in the matrix not only as individual atoms but also in the form of Al_3Er phase. In Fig. 5c, a large number of dislocations are accumulated around the Al_3Er phases. This phenomenon originates from the incorporation of element Er into the matrix during fabrication, coupled with thermal stress created inside the material during the LPBF process. When the Al_3Er phase is formed, the matrix around the Al_3Er phase experiences greater stress in the thermal cycling process due to the relatively large difference in thermal expansion coefficients between Al_3Er and the matrix. These thermal and residual stresses lead to the generation and proliferation of dislocations, which are accumulated around the Al_3Er phases. This is because of the dislocation-pinning effect of Al_3Er phase, making it difficult for the dislocation to escape from the Al_3Er phases. It is found that the element Sc forms Al_3Sc phases, with extensive dislocations accumulated around them during the formation process. This suggests that both Al_3Sc and Al_3Er can accumulate and pin dislocations. Furthermore, EDS mapping shows that TiB_2 is distributed adjacently to Sc-rich region, indicating that TiB_2 also has a certain stabilization effect on Sc.

Fig. 6 shows the favorable interface matching among Er, TiB_2, and the Al matrix. It can be seen from Fig.6a that the Er reacts with Al matrix to form Al_3Er. The lattice constant of Al_3Er is 0.4215 nm, while that of the Al matrix is 0.4043 nm, resulting in a lattice mismatch of only 4.1%. As shown in Fig.6d, the lattice constant of TiB_2 is 0.3028 nm, with a lattice mismatch of only 25.2% relative to the Al matrix. This demonstrates that Er and TiB_2 can achieve favorable interface matching with the Al matrix through direct and indirect interactions, respectively. Such good interface compatibility enhances the heterogeneous nucleation efficiency of the reinforcing phases, especially for Er and TiB_2, which is crucial for improving material properties[16]. Additionally, the dispersed distribution of Er and TiB_2 within the matrix complicates the interface network, thereby contributing to enhancement of the mechanical properties of the material.

3.3 Mechanical properties

Tensile tests were performed on the two alloys, and the results are shown in Fig. 7. Compared with Al-Mn-Mg-Sc-Zr alloy, the Er-TiB_2/Al-Mn-Mg-Sc-Zr alloy exhibits a 13.4% increment in tensile strength and a 26.4% increment in elongation. This is because the addition of Er forms many nano-sized Al_3Er phases in the aluminum matrix. These fine compounds will hinder the movement of dislocations inside the aluminum matrix and induce the accumulation of dislocations around them, further restricting the movement of other dislocations. Additionally, Al_3Er also acts as a heterogeneous nucleating agent during the solidification process of the molten pool, promoting the nucleation and growth of α-Al grains and thereby achieving grain refinement. The addition of TiB_2 particles optimizes the temperature gradient, improves the laser absorption efficiency of aluminum matrix, promotes the precipitation of secondary phase, and facilitates the heterogeneous nucleation, collectively contributing to the formation of an excellent microstructure. Therefore, the mechanical properties are greatly improved. Based on this study, the properties of the current aluminum alloy materials are compared. The fracture morphologies of the two alloys are depicted in Fig. 8. The

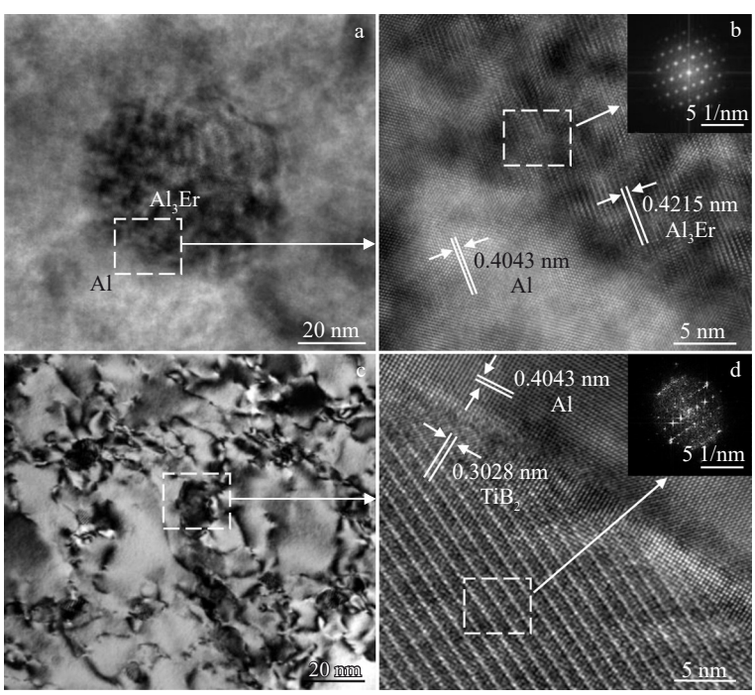

Fig.6 Lattice matching between Er and Al interface (a–b) as well as TiB_2 and Al interface (c–d)

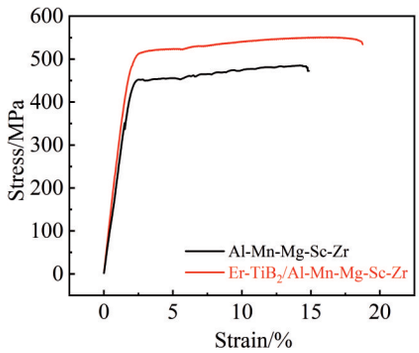

Fig.7 Stress-strain curves of Al-Mn-Mg-Sc-Zr and Er-TiB_2/Al-Mn-Mg-Sc-Zr alloys formed by LPBF

fracture surface of the Al-Mn-Mg-Sc-Zr alloy exhibits a combination of cleavage and dimple features (Fig. 8a), indicating a mixed fracture mode encompassing both ductile and brittle characteristics. In the locally magnified image (Fig. 8b), the quantity and size of dimples are small, confirming a quasi-brittle fracture behavior with limited toughness. In contrast, the fracture surface of the Er-TiB_2/Al-Mn-Mg-Sc-Zr alloy (Fig.8c) is dominated by dimples without any cleavage facets. Higher-magnification observation (Fig.8d) reveals that these dimples are larger and deeper than those in the Al-Mn-Mg-Sc-Zr alloy, showing a ductile fracture mode, which reflects the excellent toughness of the alloy. These observations from the fracture morphology are consistent with the elongation results.

3.4 Strengthening mechanisms

(1) Hall-Petch strengthening

The Hall-Petch strengthening mechanism in materials is because the greater the number of grains, the more the grain boundaries. In the solidification process, adjacent grains will squeeze each other due to the interaction forces generated by grain growth, resulting in plastic deformation. Dislocations form inside the grains, slipping and multiplying along the crystal planes, and thereby creating a stress field near the grain boundaries. Grain refinement enhances material strength by increasing the number of grain boundaries, which effectively hinders dislocation motion[17]. The longitudinal sections of Al-Mn-Mg-Sc-Zr and Er-TiB_2/Al-Mn-Mg-Sc-Zr alloys are shown in Fig.9.

(2) Solid solution strengthening

In the Al-Mn-Mg-Sc-Zr alloy, some Mn and Mg atoms will dissolve into the aluminum matrix, where they exert a pinning effect on dislocations, impeding the dislocation movement and thus increasing the alloy ' s strength. During the forming

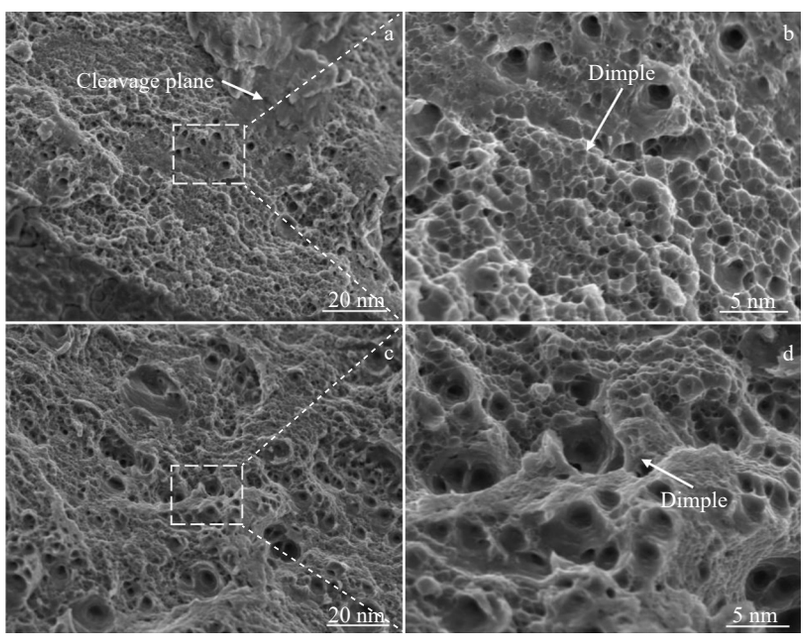

Fig.8 Fracture morphologies of Al-Mn-Mg-Sc-Zr (a–b) and Er-TiB_2/Al-Mn-Mg-Sc-Zr (c–d) alloys formed by LPBF

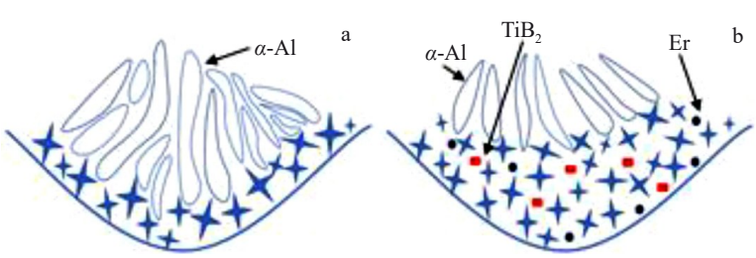

Fig.9 Schematics of longitudinal sections of Al-Mn-Mg-Sc-Zr (a) and Er-TiB_2/Al-Mn-Mg-Sc-Zr (b) alloys formed by LPBF

process, the Sc, Er, and TiB_2 will precipitate to form secondary phases that do not dissolve in the aluminum matrix. The content of the element Zr is very low, so only the solid solution strengthening of elements Mn and Mg is considered[18].

(3) Orowan strengthening

The obstruction of dislocation movement by dispersed nanoparticles in the material can enhance its strength, and this strengthening mechanism is called dispersion strengthening (or Orowan strengthening). Due to the presence of Sc in both the base material and the composites, the Sc-containing phases are not the primary focus for the discussion of the Orowan strengthening mechanism in this research. Therefore, dispersion strengthening effect refers specifically to that caused by TiB_2 and Er nanoparticles. TiB_2 and Er achieve the strengthening effect by pinning dislocations within grains and at grain boundaries. The strengthening and toughening mechanisms of Er and TiB_2 are shown in Fig.10[19].

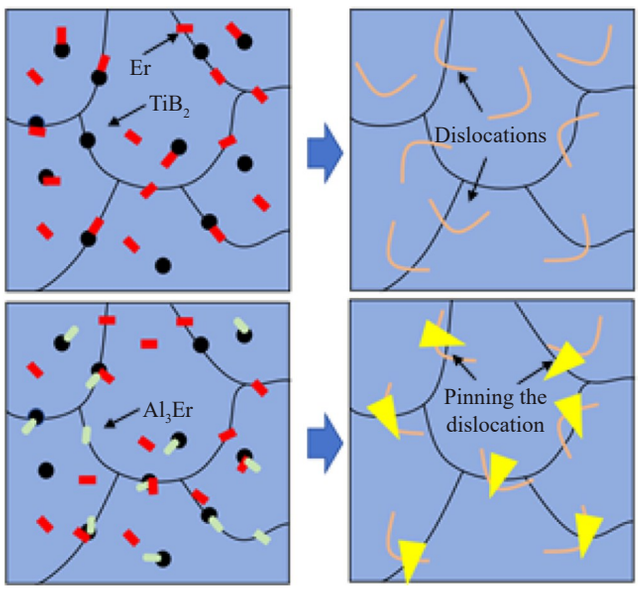

Fig.10 Strengthening and toughening mechanisms of Er-TiB_2/Al-Mn-Mg-Sc-Zr alloy[19]

(4) Load-bearing reinforcement

In the composite material, as depicted in Fig. 11, TiB_2 and Er are evenly distributed throughout the matrix. A strong interfacial bonding exists between the reinforcing phases and the matrix, enabling effective load transfer. Under tensile loading conditions, the softer Al matrix transfers load to the harder reinforcing phase particles, thereby enhancing the mechanical properties of the material. As shown in Fig.11, the cellular network structure is clear, continuous, and dense, with the reinforcing particles well-integrated into their surrounding matrix[9].

(5) Dislocation density reinforcement

As seen in Fig. 12, significant dislocation accumulation occurs in the Er-TiB_2/Al-Mn-Mg-Sc-Zr alloy. The formation of dislocations in the alloy is attributed to not only the thermal stress induced by rapid cooling during the forming process, but also the mismatch in thermal expansion coefficients between the reinforcing phase and the matrix[20].

3.5 Toughening mechanism

Based on the experimental results, the elongation at break

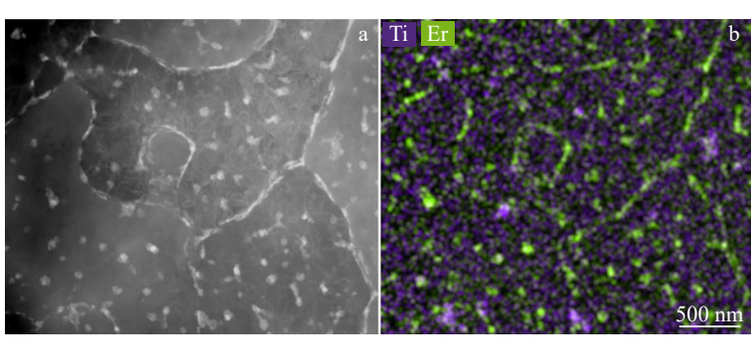

Fig.11 Interface bonding of Er-TiB_2/Al-Mn-Mg-Sc-Zr alloy (a) and corresponding EDS mapping (b)

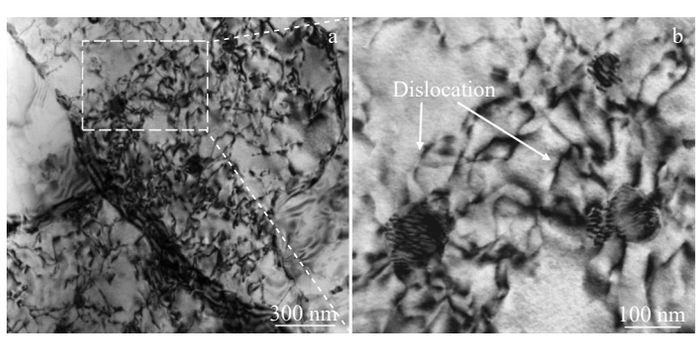

Fig.12 Internal dislocation distributions in grains of Er-TiB_2/Al-Mn-Mg-Sc-Zr alloy

and the tensile strength of the dual-phase composite can reach a maximum of 18.7% and 550 MPa, respectively. Generally, the improvement in tensile strength is often accompanied by a sacrifice in toughness. For nanocomposites, however, the good interfacial bonding between the reinforcing phase and the matrix, as well as the grain refinement effect, can alleviate this trade-off.

Grain refinement can enhance ductility. As the grains are refined, columnar grains are gradually transformed into equiaxed grains. The total number of grains increases, and consequently, the grain boundaries increase as well. The stress concentration borne by individual grains is reduced and can be released over time, which decreases the possibility of crack nucleation. Randomly oriented equiaxed grains are beneficial to the improvement of plasticity. During the tensile deformation of columnar grains, local strain makes it difficult to release stress concentration, increasing the likelihood of crack generation. In contrast, non-oriented equiaxed grains are subjected to uniform stress, reducing local strain. Meanwhile, the deformation coordination ability is enhanced, and the relatively low stress concentration can be released over time, thereby achieving more uniform plastic deformation and increasing the elongation at fracture. Therefore, grain refinement is one of the key reasons for the increase in elongation at break.

The distribution of the reinforcing phase is another important factor influencing the elongation at break. Experiments show that the reinforcing phase particles are discretely distributed both intragranularly and intergranularly, and these particles are well bonded to the matrix. The lattice constants of Al_3Er and the aluminum matrix are highly similar, and there is good atomic coordination between them. When the material is subjected to external forces, load can be more effectively transferred from the matrix to the Al_3Er phase. When the lattice constants of the precipitated phase are close to those of the aluminum matrix, the interfacial lattice mismatch is very small. A small lattice mismatch means minimal stress generated due to lattice distortion at the interface between the Al_3Er phase and the aluminum matrix. Such a low-stress interface can effectively prevent the initiation and propagation of cracks at the interface. Since the generation and propagation of cracks typically need to overcoming specific energy barriers, the low-stress interface reduces the driving force for crack formation, thereby improving the toughness of the material. While causing a dislocation-pinning effect within the microstructure, the reinforcing phases are closely combined with the matrix, hindering the grain growth. Most cracks are suppressed by the reinforcing phases, and the fracture is mainly dominated by dislocation activity. Therefore, the increase in elongation at break of nanocomposites can be attributed to the inhibitory effect of the reinforcing phases on cracks.

4 Conclusions

1) The addition of Er in the Al-Mn-Mg-Sc-Zr alloy leads to the formation of fine Al_3Er phases through reaction with the matrix. The addition of TiB_2 can optimize the influence of temperature gradients in the forming process and promote the precipitation of more secondary phase.

2) In the Er-TiB_2/Al-Mn-Mg-Sc-Zr alloy, the grains exhibit obvious refinement, and the texture strength tends to weaken. This indicates that the addition of reinforcing phase refines the grains and reduces the anisotropy caused by temperature gradients during the LPBF forming process. Consequently, the multidirectional growth of grains is enhanced.

3) The Er-TiB_2/Al-Mn-Mg-Sc-Zr alloy achieves a tensile strength of 550 MPa and an elongation at break of 18.7%. Compared with those of the Al-Mn-Mg-Sc-Zr alloy, both the strength and plasticity are significantly improved. The strengthening mechanisms underlying the enhanced mechanical properties of the Er-TiB_2/Al-Mn-Mg-Sc-Zr alloy are analyzed.

References

1 Sitek J, Degmová J. *Hyperfine Interactions*[J], 2006, 165(1–4): 121

2 Kotadia H R, Gibbons G, Das A *et al*. *Additive Manufacturing*[J], 2021, 46: 102155

3 Chen Jiwei, Xiong Feiyu, Huang Chenyang *et al*. *Scientia Sinica Physica*[J], 2020, 50(9): 104

4 Zhang Changchun, Zhu Haihong, Qi Yang *et al*. *IOP Conference Series: Materials Science and Engineering*[J], 2019, 538: 12023

5 Zhang D Y, Arvind P, Michael J B *et al*. *Metallurgical and Materials Transactions A*[J], 2020, 51(9): 4341

6 Adriaan B S, Karl D, Mark V *et al*. *CIRP Annals*[J], 2016, 65: 213

7 Li Ruidi, Chen Hui, Zhu Hongbin *et al*. *Materials & Design*[J], 2019, 168: 107668

8 Li X P, Ji G, Chen Z *et al*. *Acta Mater*[J], 2017, 129: 183

9 Shi Jinglin, Hu Qiang, Zhao Xinming *et al*. *Transactions of the Indian Institute of Metals*[J], 2023, 76(6): 1605

10 Martin J H, Yahata B D, Hundley J M *et al*. *Nature*[J], 2017, 549(7672): 365

11 Wang Junhao, Zhao Jibin, He Chen *et al*. *Rare Metal Materials and Engineering*[J], 2024, 53(12): 3485 (in Chinese)

12 Booth-Morrison C, Seidman D N, Dunand D C. *Acta Mater*[J], 2012, 60(8): 3643

13 Wang P, Gammer C, Brenne F *et al*. *Composites Part B*[J], 2018, 147: 162

14 Ziemnicka-Sylwester M. *Materials*[J], 2013, 6(5): 1903

15 Wu Min, Tao Jing, Wang Jihao *et al*. *Journal of Materials Research and Technology*[J], 2023, 23: 3537

16 Li Min, Yao Sen, Wang Jiajian *et al*. *Journal of Materials Research and Technology*[J], 2022, 20: 2021

17 Chen Fei, Chen Zongning, Mao Feng *et al*. *Materials Science and Engineering A*[J], 2015, 625: 357

18 Øyvind R, Oscar N, Emmasjo L *et al*. *Metallurgical and Materials Transactions A*[J], 2006, 37(6): 1999

19 Liu G, Zhang G J, Jiang F *et al*. *Nature Materials*[J], 2013, 12(4): 344

20 Sanaty-Zadeh A. *Materials Science and Engineering A*[J], 2012, 531: 112

添加 Er-TiB_2双相纳米颗粒对激光粉末床熔融制备 Al-Mn-Mg-Sc-Zr 合金强度-韧性的影响

李素丽[1]，张晏泽[1]，杨蒙佳[1]，张龙博[1]，谢启东[2]，杨来侠[1]，毛　丰[3]，陈　祯[2]

(1. 西安科技大学 机械工程学院，陕西 西安 710054)

(2. 西安交通大学 机械工程学院，陕西 西安 710049)

(3. 龙门实验室，河南 洛阳 471000)

摘　要：采用双相协同增强的方法，利用Er和TiB_2的特有优势对激光粉末床熔融（LPBF）制备的Al-Mn-Mg-Sc-Zr合金进行强化。采用真空均质技术制备了0.5wt% Er-1wt% TiB_2/Al-Mn-Mg-Sc-Zr纳米复合材料的球形粉末，LPBF工艺制备的样品密度达到99.8%。探讨了Er-TiB_2的强化机理和增韧机理。结果表明，XRD分析存在Al_3Er衍射峰，EBSD结果显示双相纳米颗粒添加后合金织构强度下降。添加的Er和TiB_2纳米增强相在LPBF形成过程中起非均相形核作用，阻碍晶粒长大，可有效细化晶粒。添加Er和TiB_2双相纳米增强相后，LPBF成形样品的抗拉伸强度和延伸率分别达到550 MPa和18.7%，相较基体材料提高13.4%和26.4%。

关键词：Al-Mn-Mg-Sc-Zr合金；激光粉末床熔融；纳米增强相；协同增强

作者简介：李素丽，女，1981年生，博士，副教授，西安科技大学机械工程学院，陕西 西安 710054，E-mail：Lty15802949318@xust.edu.cn